

Article

Experimental Study of Confined-Pressure Soaking on Sandstone Damage-Fracture Characteristics Using Acoustic Emission and Energy Dissipation

Baobao Chen ^{1,2,*} , Lei Wang ¹  and Ming Zhang ¹ 

¹ State Key Laboratory of Mining Response and Disaster Prevention and Control in Deep Coal Mines, Anhui University of Science and Technology, Huainan 232001, China

² School of Civil Engineering, Shandong Jianzhu University, Jinan 250101, China

* Correspondence: cbb@aust.edu.cn; Tel.: +86-198-5540-3998

Abstract: In order to explore the mechanical characteristics of confined-pressure soaking (CPS) sandstone during the damage-fracture process, the uniaxial compression and acoustic emission (AE) experiment of CPS sandstone was conducted. The mechanical parameters, fracture morphology, AE and energy characteristics under uniaxial stress were researched. The results show that the uniaxial compressive strength and elastic modulus decrease as a logarithmic function with CPS parameters, corresponding to the inflection point of modification. The fracture mode gradually changes from brittleness to toughness with the increase in moisture content. The difference between fracture fragmentation and mechanical behavior mainly depends on the degree of CPS. The evolution of AE characteristics and energy dissipation has a good correspondence with CPS specimens. The higher the CPS degree is, the less the AE cumulative number is and the longer the excitation time is. Based on the phase variation of AE events and energy dissipation, the CPS damage variables are proposed to quantify the weakening degree and reveal the damage evolution process. The results provide a useful foundation for evaluating rock failure and improving service life.

Keywords: confined-pressure soaking (CPS); mechanical characteristics; fracture morphology; acoustic emission; damage evolution



Citation: Chen, B.; Wang, L.; Zhang, M. Experimental Study of Confined-Pressure Soaking on Sandstone Damage-Fracture Characteristics Using Acoustic Emission and Energy Dissipation. *Sustainability* **2022**, *14*, 12381. <https://doi.org/10.3390/su141912381>

Academic Editors: Cun Zhang, Fangtian Wang, Shiqi Liu and Erhu Bai

Received: 28 July 2022

Accepted: 23 September 2022

Published: 29 September 2022

Publisher's Note: MDPI stays neutral with regard to jurisdictional claims in published maps and institutional affiliations.



Copyright: © 2022 by the authors. Licensee MDPI, Basel, Switzerland. This article is an open access article distributed under the terms and conditions of the Creative Commons Attribution (CC BY) license (<https://creativecommons.org/licenses/by/4.0/>).

1. Introduction

At present, confined-pressure water blasting technology is one of the effective measures for pre-splitting hard roofs and preventing rockburst in coal mines in China [1]. Coupling blasting with confined pressure water is to fill the borehole with water instead of air and the surrounding rock could reach a specific soaking time in the state of pressure stabilization. Then the charge initiates to achieve a better fracturing effect. The drilling fractured rock mass forms a certain range of immersion zone, and meanwhile, the soaking range and degree will be further strengthened under the effect of confined-pressure increasing permeability, so as to obtain a large range of soaking modified rock mass [2–4]. The time and pressure change of confined-pressure water soaking (CPS) stimulates the response of rock mass to varying degrees (moisture content), inducing the microstructure modification of rock mass [5–7]. Therefore, it is of great significance for rock stability monitoring and disaster early warning in coal mine production to master the characteristics of deformation and failure precursory indicators of CPS rock [8].

After loading, the crack closure and secondary propagation of rock mass will be accompanied by the release of elastic wave, which propagates rapidly and produces acoustic emission (AE) events [9]. Therefore, understanding the AE characteristics of rock is helpful to master the law of crack propagation and damage evolution. There is an internal relationship between the mechanical characteristics and AE damage, and the confined-pressure water will weaken the rock samples, affecting the relationship between

the parameters [10]. As for the influence of water on rock weakening, scholars have done a lot of research and achieved some research results. Yao et al. [11] proposed the new Mohr-Coulomb model of coal samples with various moisture content and analyzed the effect of water level on the tensile failure planes as well as the percentage of tensile failure planes versus the total. The increasing moisture content promotes the possibility of shear failure. The weakening degree mainly depended on the clay mineral content [12]. Zhang et al. [13] pointed out AE activities could be divided into compaction and elastic deformation, non-elastic deformation and fracturing failure phase and proposed a new damaged model to describe the coal damage. Qin et al. [14] carried out the uniaxial compression mechanical and AE tests of rock samples with different moisture content and clarified the influence of moisture content on AE characteristics. Teng et al. [15] analyzed the mechanical and AE characteristics of dry and saturated sandstone under different loading rates. The constitutive model was proposed and confirmed based on the softening factors of elastic modulus (EM). Geng et al. [16] pointed out a gradual change of the sandstone deformation mode from brittle to ductile with moisture content increasing. Based on AE accumulative and dissipated energy theory, damage variables were proposed which could reflect the damage evolution during the compression. Cai et al. [17,18] analyzed the influence of water saturation on the mechanical behavior of different rock types, obtaining the influence characteristics of immersion on the strain, uniaxial compressive strength (UCS) and EM. The weakening degree depended on the porosity and content of the expansive clay. Shen et al. [19] found that water reduced the strength and brittleness of coal by destroying the microstructure and resulting in elastic energy accumulation. Zhu et al. [20] explored the crack activity of saturated rocks at key stress points by uniaxial compression and AE tests. The results showed due to the existence of water, the number of AE events decreased relatively, indicating that water enhanced the ductility. Qin et al. [21] analyzed the compression failure characteristics of coal samples and obtained the response of strength and AE characteristics to moisture content. The increase in moisture content resulted in a decrease in AE accumulation and an increase in excitation time lag. Xia et al. [22] carried out experimental research on AE characteristics during cyclic loading and unloading of dry-saturated rock.

To sum up, the stress-strain behavior, fracture mode, energy and AE characteristics of rock are sensitive to water immersion, and the weakening degree of for different types of rock mainly depends on the content of expansive clay. The literature research mainly focuses on the weakening damage effect on rock, with natural soaking time and moisture content as the influencing factors. Compared with natural soaking, the weakening effect of confined-pressure water is different in that confined-pressure water activates the propagation of micro-cracks, and further strengthens the modification of rock. There are few studies on the response of mechanical and acoustic characteristics of modified sandstone by confined-pressure water to the soaking time. In addition, the influence of confined-pressure variation on the damage characteristics of sandstone has not been reported, and the mechanism of confined-pressure water and rock interaction during loading is unable to verify. Therefore, it is the feature of the research to effectively correlate CPS parameters with sandstone damage (based on AE and energy dissipation).

Therefore, taking the sandstone roof of Datong Mining Area as the research object, uniaxial compression tests were carried out on the soaking specimens through MTS and AE test systems. The stress-strain curves, mechanical properties, fracture morphology, AE events and energy were closely linked together, and the geometric relationship with CPS parameters was established. Then, from the point of view of the phased characteristics of AE events and the evolution of energy dissipation, the damage evolution characteristics of CPS sandstone at different loading stages are quantified. The damage variables under different CPS degree are derived and established, and the applicability is obtained. Combined with the engineering environment of confined pressure blasting in a coal mine, the work comprehensively explored the evolution characteristics of the sandstone mechanical

damage under different CPS parameters and their quantitative relationship, so as to better apply it to coal mine safety production.

2. Test Scheme

2.1. Sandstone Specimens Preparation

The testing core was taken from the main roof of 8939 working face in Xinzhouyao mine of Datong Mining Area, China. The integrated core and drilling borescope were shown in Figure 1. The surface of sandstone is grey, and joint characteristics are not significant. According to GB/T23561.7-2009 “Methods for determining the physical and mechanical properties of coal and rock”, the rock was processed into cylinders perpendicular to stratification with dimensions of $\Phi 50 \times 100$ mm. The average mass of the rock sample is 494.5 g, and the average natural density is 2526 kg/m^3 . The irregularity error of ends was controlled within 0.05 mm to ensure good contact between the tester and specimen ends. The specimens with obvious appearance defects were removed, and the longitudinal wave velocity of the samples was measured (average value was 2641 m/s). Rock blocks with similar wave velocity were selected as the experimental reserves.

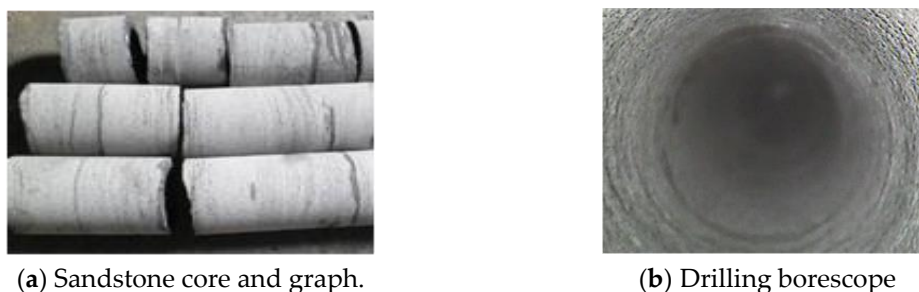


Figure 1. Selection of sandstone core.

The sample was analyzed by XRD, and the diffraction pattern is shown in Figure 2.

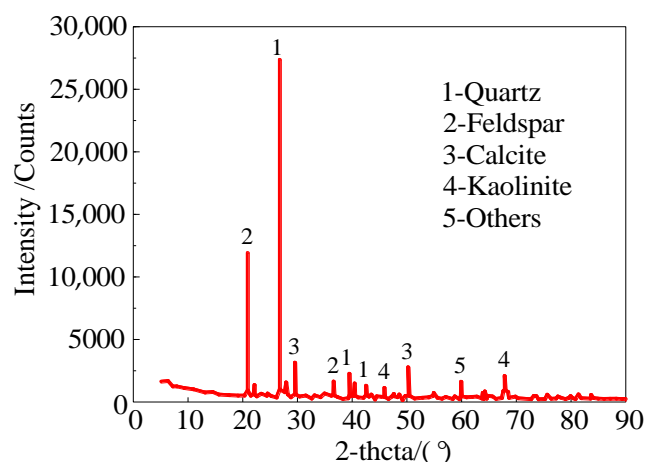


Figure 2. X-ray diffraction figure of mineral composition of sandstone.

The content of quartz and feldspar in sandstone is the highest, followed by calcite, and the least is kaolinite, among which kaolinite is greatly affected by water soaking. Kaolinite has strong water absorption and has expansion and plasticity after soaking. Because the content of kaolinite is relatively low, the soaking and modification effect of sandstone will be lower than that of mudstone or argillaceous siltstone.

2.2. Testing Instrument and Parameter Design

Before loading, the independent design and detachable CPS device were used to realize the different CPS degrees of specimens, as shown in Figure 3.

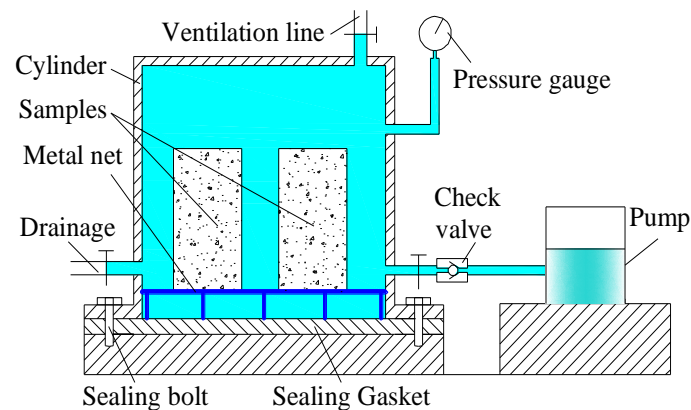


Figure 3. Confined-pressure soaking device for coal-rock.

Before conducting the experiment, the sealing chamber is opened to place the specimens on the loading platform, and then the device is reassembled and sealed. The water is injected into the cavity through the pump and water injection to soak the rock sample until the cavity is full. In the simulation of the CPS environment, the pressure relief valve and pressure gauge monitoring are used to achieve the specific soaking time of samples under different stable CPSPs.

AE monitoring adopts the PCI-2 acquisition system, and relevant parameter settings are shown in Table 1. Paste the strain gauge and AE sensors (piezoelectric AE sensor Nano30, bandwidth 125~750 KHz, resonant frequency 140 KHz) according to Figure 4. After connecting the corresponding equipment with the acquisition system, it is necessary to conduct several sets of broken-lead experiments to ensure that each sensor is in the best coupling state with the rock sample surface. Only in this way could the AE sensor stably receive high-quality signals during the experimental process.

Table 1. Parameter setting of AE acquisition system.

Threshold/dB	Sampling Rate/MHz	Pre-trigger/ μ s	Peak Definition Time (PDT)/ μ s	Hit Definition Time (HDT)/ μ s	Hit Locking Time (HLT)/ μ s
40	5	256	50	200	300

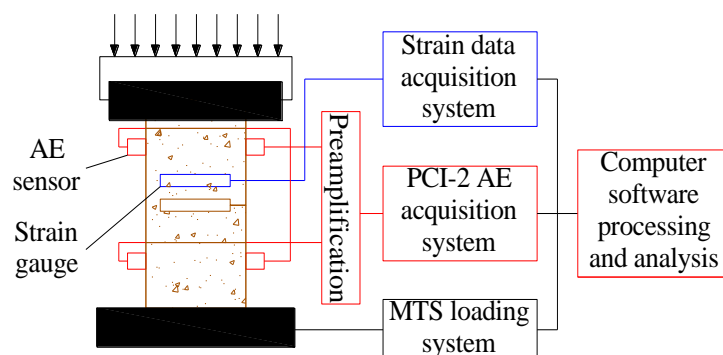


Figure 4. Test system of uniaxial compression and AE monitor for CPS sandstone.

CPS specimens were loaded by an electro-hydraulic servo universal tester with a displacement loading rate of 0.5 mm/min. The stress-strain data acquisition system used a static strain gauge, displacement sensor and stress sensor to monitor the deformation and loading of specimens. Combined with the actual production, it was determined that the confined-pressure soaking time (CPST) of rock specimens was 0~24.0 h and confined-pressure soaking pressure (CPSP) was 0~8.0 MPa.

3. Results and Analysis

3.1. Mechanical Characteristics of CPS Sandstone

The sandstone contains water-absorbing minerals such as clay, which makes the moisture content increase continuously and micro-structure modification. Especially for CPS, the degree of modification and weakening is enhanced [23]. In order to analyze the mechanical properties under different CPS degrees, the moisture content is measured, and the sensitive range of influencing factors on modification is analyzed. Meanwhile, the uniaxial compression test is carried out to explore the response characteristics of UCS and EM to CPS parameters.

3.1.1. Analysis of Characteristics of Soaking Degree for Sandstone

The variation curves of moisture content under different CPS degrees are shown in Figure 5.

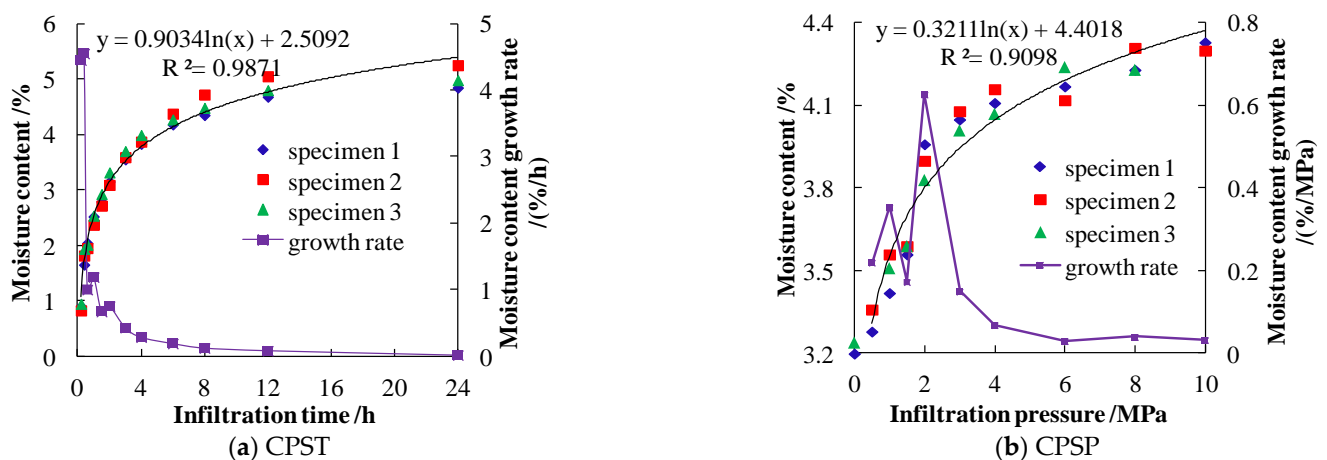


Figure 5. Moisture content variation under different CPS degrees.

The moisture content of CPS specimens shows the characteristics of stage growth. For CPST, the main growth stage is 0~12.0 h with the rate gradually decreasing, which indicates the water absorption-dissolution-modification process is basically completed within 12.0 h. For CPSP, the main growth stage is 1.0~6.0 MPa (main stage: 1.5~3.0 MPa), during which CPS has a significant effect on micro-modification. In other words, the permeability and mudding resistance are the most significant in 1.5~3.0 MPa. When the pressure exceeds 6.0 MPa, the response of moisture content to CPSP decreases obviously.

The variety of moisture content could indirectly reflect the response of modification intensity to CPS degree of sandstone. Therefore, the factor interval (CPST: 0~24.0 h, CPSP: 0~6.0 MPa) affecting the modification degree is determined.

Because the moisture content increase in sandstone caused by CPS is different from that of the natural soaking, in order to verify the reliability of the test conclusion and innovation, the paper compares the change of moisture content by CPS with that in the relevant literature. The natural moisture content satisfies a variety of positive correlation functions in terms of soaking time [24,25], while the moisture content induced by CPST in the paper satisfies a logarithmic function. Taking red sandstone as an example [26], the increase in moisture content obtained by comparing CPS is shown in Equation (1). However, the changing trend of the moisture content for natural and CPS is similar, which could be approximately divided into three stages and the growth rate of each stage is consistent [27,28].

$$\begin{cases} \text{CPST} : w_t = 0.9034 \ln(t) + 2.5092 \\ \text{Natural} : w_t = -4.26e^{-t/7.2} + 4.27 \end{cases} \quad (1)$$

where, t is the soaking time, including natural and CPS state; w_t is the moisture content. The formula could be used for forecasting the moisture content through the soaking time.

For the increase in CPSP, the moisture content increase in the soaking process is similar to that of the CPST state. Therefore, the conclusion obtained based on CPS parameters is consistent with the previous research, indicating the reliability of the experimental conclusion.

3.1.2. Mechanics Characteristics of Sandstone under Different CPS Degree

The stress-strain curves of specimens under different CPSTs are shown in Figure 6.

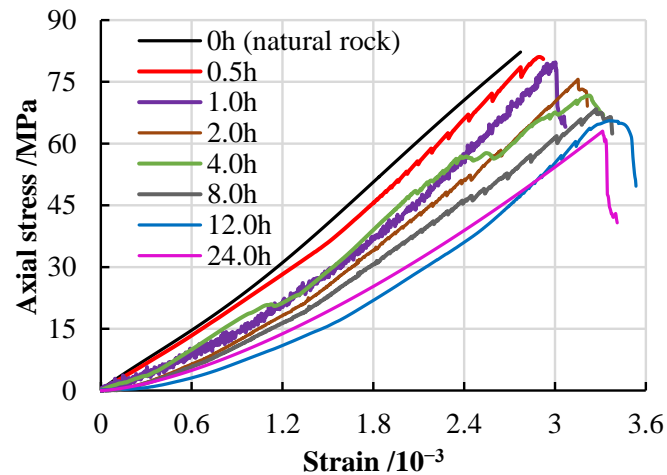


Figure 6. Stress-strain curves under different CPSTs.

CPST has a certain influence on the loading process of the specimens. For the natural sandstone, the stress-strain curve increases approximately linearly without an obvious yield stage, showing brittle fracture. With the increase in CPST, the crack initial-closure section of loading specimens grows, which indicates that CPST increase activates the development of primary cracks. The middle of the curve shows “lower convex” and the nonlinear deformation period of the natural samples is shorter than that of CPS samples, showing the transition from the elasticity of natural specimens to the non-linear loading of CPS specimens. After peak stress, the specimens show a sudden drop-transition decline, and some have the post-peak bearing capacity, which indicates that the failure of specimens gradually transit from brittle to non-brittle.

Variations of UCS and EM under different CPSTs are shown in Figure 7.

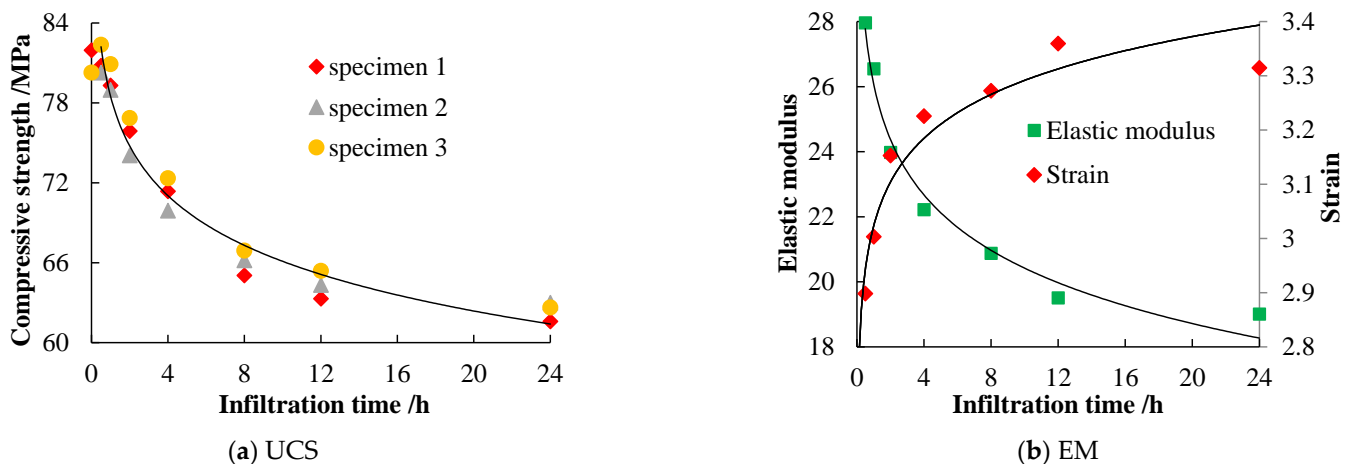


Figure 7. Mechanical parameters variation with different CPST.

With the increase in CPST, UCS and EM decrease in the form of logarithmic function and the various trend is similar, which is in good agreement with the change of moisture content. The rapid attenuation stage is 0~8.0 h, corresponding to UCS decreasing from

82.24 MPa to 66.04 MPa (EM: 29.66 GPa to 20.88 GPa). Compared with natural specimens, UCS and EM are reduced with 21.0% and 29.6%, respectively. The attenuation rate obviously decreases in 8.0~24.0 h, and UCS and EM are reduced with 27.0% (UCS) and 36.0% (EM), respectively. The failure strain corresponding to UCS increases, and the attenuation strength of EM is higher than that of UCS, which indicates that the failure of specimens transit from brittleness to non-brittleness. Based on the attenuation trend of UCS and EM, the sensitive CPST range of weakening is 2.0~8.0 h.

The stress-strain curves of specimens under different CPSP are shown in Figure 8.

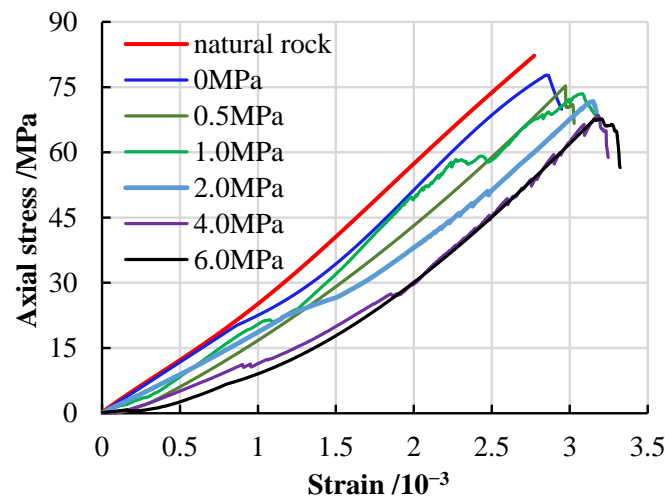


Figure 8. Stress-strain curves of specimens under different CPSP.

The variation of the stress-strain curves on the CPSP is similar to that of CPST, presenting “lower convex” growth as a whole. With the increase in CPSP, the crack closure process increases (the growth stage of CPSP is lower than that of CPST, that is, the crack activation and propagation degree decrease), and the convex bending amplitude increases. When CPSP is lower than 1.0 MPa, the stress peak has no obvious yield stage. When the CPSP exceeds 2.0 MPa, the curve has an obvious drop process, and there is no obvious post-peak bearing capacity.

Figure 9 shows the variation of UCS and EM with different CPSPs.

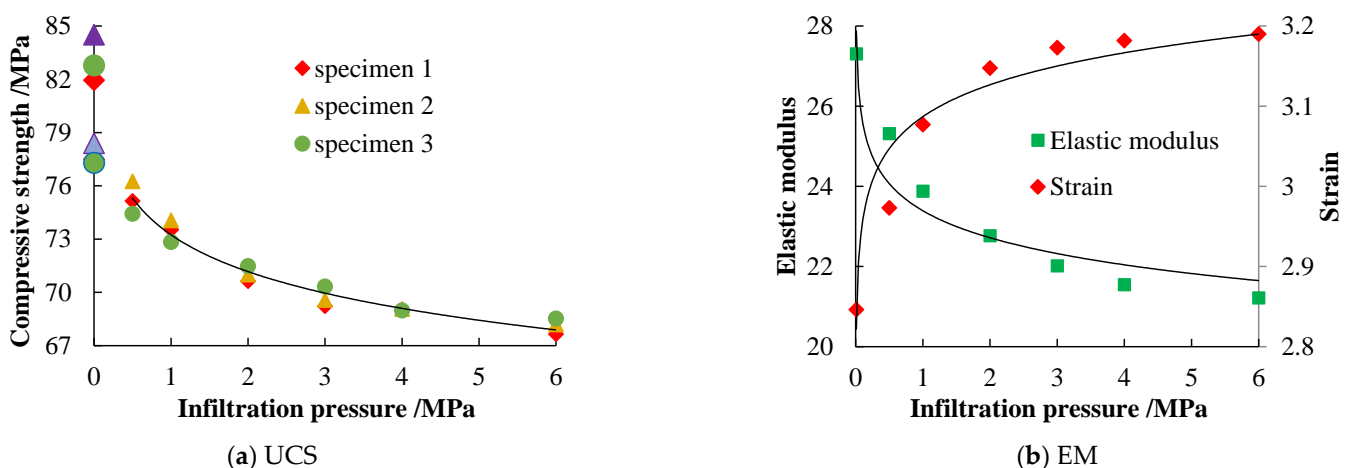


Figure 9. Mechanical parameters variation with different CPSP.

The attenuation law of UCS and EM on CPSP is similar to that of the CPST in logarithmic function, which is in good agreement with the moisture content. The attenuation could be divided into three stages: when CPSP is lower than 2.0 MPa, UCS decreases from 82.24 MPa (natural) to 71.04 MPa (29.66 GPa to 22.02 GPa for EM), which is 13.6% and

23.2% lower than that of the natural. The attenuation degree decreases at 2.0~4.0 MPa with 16.1% and 27.3% (UCS and EM) lower than that of the natural state. The UCS and EM of the specimen decreased by 17.2% and 28.5%, respectively, within 4.0~6.0 MPa. The peak strain corresponding to the peak strength shows an increasing trend, indicating that the failure of the specimen varies from brittle fracture to non-brittleness. Based on the attenuation trend of UCS and EM, the sensitive value of CPSP is determined at 2.0~4.0 MPa.

The decrease in UCS and EM is an important feature of sandstone softening under CPS. The quantitative relationship between UCS (EM) and CPST/CPSP is proposed by fitting:

$$\left\{ \begin{array}{l} t : \begin{cases} \sigma_c(t) = -5.379 \cdot \ln(t) + 78.488 \\ E(t) = -2.457 \ln(t) + 26.077 \\ \varepsilon(t) = 0.1165 \ln(t) + 3.0232 \end{cases} \\ p : \begin{cases} \sigma_c(p) = -2.99 \cdot \ln(p) + 73.243 \\ E(p) = -0.974 \ln(p) + 23.393 \\ \varepsilon(p) = 0.0575 \ln(p) + 3.0868 \end{cases} \end{array} \right. \quad (2)$$

where, $\sigma_{c(t)}/\sigma_{c(p)}$ and $E(t)/E(p)$ are UCS and EM under different CPSTs and CPSPs.

In order to illustrate softening effect of CPS on sandstone, the weakening characteristics of conventional soaking in related research are compared. In the paper, the test results are compared with the strength parameters of samples with different moisture contents, as shown in Figure 10. The curves fitted in the previous literatures are mainly negative exponential and quadratic functions [16,29–31]. Meanwhile, it is found that UCS and EM satisfy the negative logarithmic function for CPST and CPSP. For CPSP growth under a specific CPST, the mechanical parameters continue to decay, indicating that the CPS weakening is the coupling effect of soaking time and high-pressure water. The increase in CPST and CPSP are also accompanied by the continuous growth of moisture content. Therefore, the UCS and EM of the specimen decrease with the increase in moisture content [31], whether from CPS or natural soaking. The results show the reliability of the experimental data and also show the weakening effect of the confined-water and rock coupling.

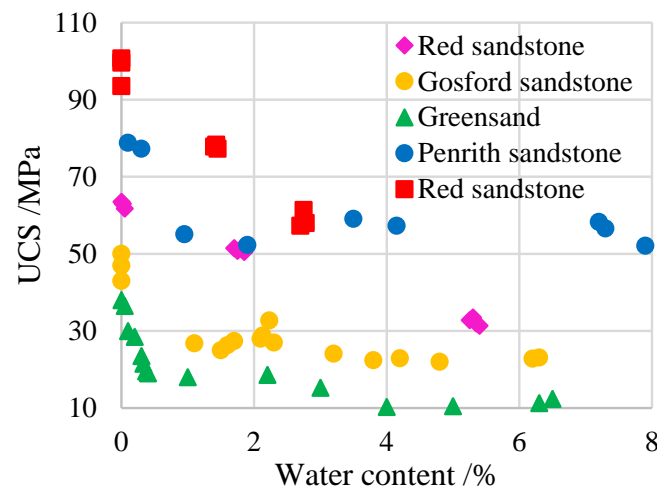


Figure 10. Variation of moisture content and uniaxial compressive strength of various sandstones.

3.1.3. Fracture Characteristics of CPS Sandstone

After CPS, minerals will be muddled, and internal micro-cracks will be activated. Meanwhile, the water absorption would cause the modification of micro-structure, and the fractures mainly propagate along the activated micro-cracks zone [32]. Failure pattern under different CPSTs is shown in Figure 11.

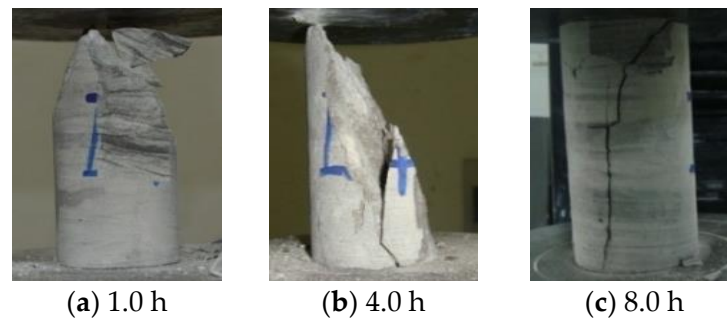


Figure 11. Failure patterns of specimens under uniaxial compression with different CPST.

With the increase in CPST, the specimens transit from local fracture to the overall. When soaking 1.0 h, the fracture is concentrated in the shallow layer of the middle and upper part, while the lower remains intact; it indicates that the short-term soaking causes the modification heterogeneity and results in the formation of local stress concentration during the loading, showing fracturing regional centralization and fragmentation irregularity. When soaking 4.0 h, the specimen shows the characteristics with the upper fracturing and the lower splitting, and the cracks penetrate along the axial direction, during which the fracture surface is irregular due to the change of fracture direction. At soaking 8.0 h, the fracture morphology of specimens is similar to that of the natural: a single main crack penetrates along the axial direction, and the fracture surface is regular, showing a homogenized strength weakening effect. The failure presents a transition to non-brittle fracture in CPST.

Figure 12 shows the fracture patterns of specimens with different CPSPs. Under low pressure (1.0 MPa), the fracture trajectory propagates irregularly, accompanied by spalling. The main crack propagates to the middle of the specimen, produces lateral rotation, and then develops stably until the specimen penetrates and ruptures, during which the main-wing cracks propagate alternately. Under 2.0 MPa, the upper part of the specimen propagates along two cracks and converges into a main crack at 3/4 height. Meanwhile, a lateral wing crack is developed in the middle of the specimen and the right side of the loading failure specimen is relatively intact, which still has high axial bearing capacity. Under the pressure of 6.0 MPa, the fracture trajectory of the specimen will show irregular development: the crack propagation has multi-directionality, presenting multiple-cracks and multiple-pieces; it indicates that when CPSP exceeds the sensitive weakening value, the fracture dimension increases; this is due to the increase in CPSP, the weakening degree of specimen increases, which is different from the homogenization weakening characteristics under CPSTs. Under a high CPSP, the internal weakening of the specimen presents multi-direction-irregularity, and the deterioration degree is more significant.

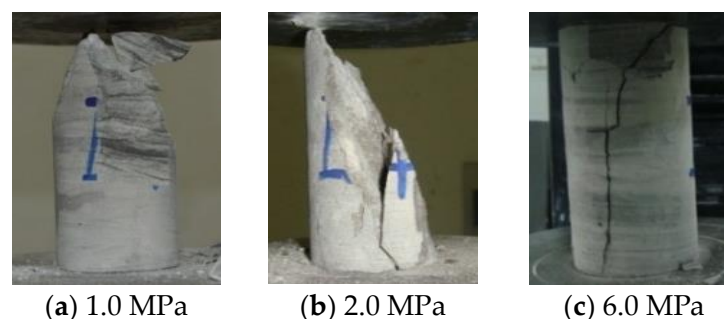


Figure 12. Fracture patterns of specimens under uniaxial compression for different CPSP.

The failure and fracture modes of CPS and natural soaking rock samples are similar with the increase in moisture content. Under three soaking conditions, the modification effect of low-medium moisture content on rock samples is mainly shear failure [33,34]. For high moisture content, the specimens subjected to CPS and natural soaking tend to be

homogeneous in modification; their fracture modes are consistent, showing longitudinal tensile cracks and local fragments [35,36]; this shows the reliability of the experimental results of the CPST effect. For high confined pressure, the modification and weakening degree of specimens increases. The specimens have a higher level of fragmentation and more small fragments are produced when a fracture occurs, which further reveals the weakening effect of confined-pressure water on sandstone; this is one of the characteristics of CPS modification and weakening.

3.2. AE Characteristics of CPS Sandstone during Loading

3.2.1. Comparison of AE Characteristics of Sandstone under Different CPS Degree

The loading specimen fracture is the combined action of the internal micro-crack closure, energy accumulation, transformation and release [37,38]. AE monitoring system could receive the signal of a damage-failure process for loading specimen, reflecting the crack propagation [39,40]. The CPS modification would inevitably lead to the change of fracture characteristics. The accumulation number of AE event is selected as a quantitative parameter for analyzing the relationship between AE signal and strain and its response to CPS degree. AE event number-strain curves with different CPSTs and CPSPs are shown in Figure 13.

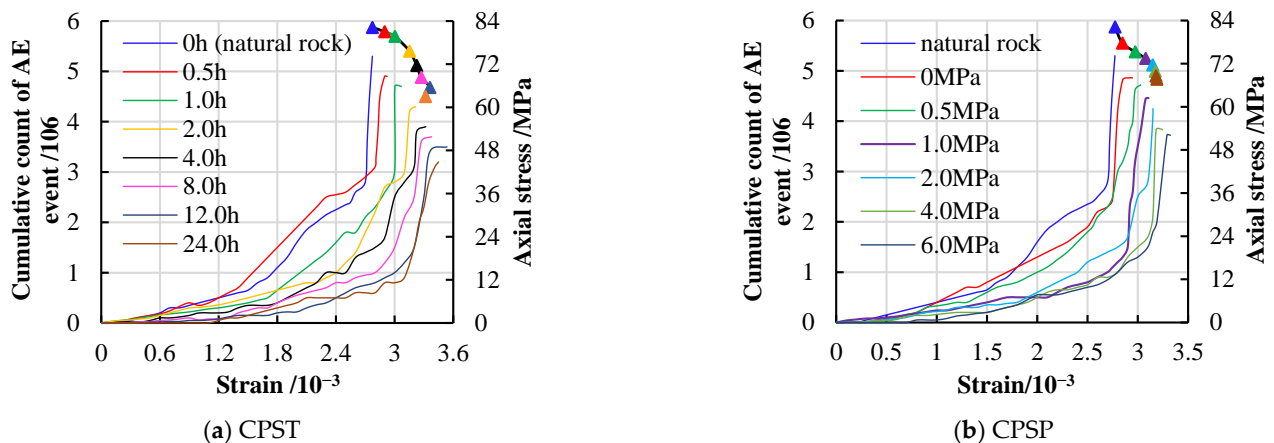


Figure 13. Accumulative number of AE events-strain curve under different CPS degree.

Combined with the stress-strain curves, it can be seen that the evolution of AE cumulative events with different CPS parameters in the loading is consistent. The variation of AE events could be divided into four stages: the first is the primary micro-fracture closure stage, in which the AE signal is very little. The second is elastic deformation, in which the cumulative number of AE events increases slowly, but the growth rate and loading duration is different under different CPS degree. The third is the rapid damage accumulative stage, and the fourth is the fracture-instability stage. With the increase in CPS degree, AE cumulative events vary from step-up to rapid growth in the stage.

In the primary fracture closure stage, AE events of all specimens is very few, but the loading strain of cracks closure stage increases. The reason is that the stress level of the specimen is low at the initial loading stage, and the primary crack is mainly compacted and closed without crack propagation. With the increase in CPS degree, the intensity of mudding and micro-structure modification increases, and the corresponding number of micro-cracks propagation decreases, resulting in the corresponding strain increasing.

The second stage is the elastic deformation, in which AE event accumulation number shows a stable increase. CPS sandstone is mainly elastic deformation without obvious damage-failure characteristics. With the increase in CPS degree, AE accumulation number shows a lower trend. Especially when CPST is more than 8.0 h and CPSP exceeds 2.0 MPa, the attenuation trend decreases obviously. The response of AE accumulation number to CPST is more sensitive in the stage.

The third stage is damage accumulation stage, including crack initiation-propagation and damage accumulation precursor before fracture. For crack initiation, AE event rate increases significantly, and the number fluctuates significantly, which corresponds to the initiation, propagation and even penetration of internal cracks. With the increase in CPS degree, AE event rate decreases gradually, indicating that confined water softens sandstone and indirectly inhibits AE event generation. For the damage accumulation precursor stage before fracture, with the increase in CPS degree, the weakening effect of sandstone is strengthened. At the stage, AE event rate increases sharply with the strain inflection point of 85~95%, but the peak value gradually decreases with local abrupt changes.

The fourth stage is the fracturing instability. For natural samples, the failure presents brittleness characteristics without obvious post-peak characteristics. With the increase in CPS degree, the strain increases continuously after fracturing, but the AE accumulation number no longer increases, that is, the softening of CPS sandstone makes no crack propagation in the instability stage, and almost no AE signal occurs.

The increase in CPS degree has obvious inhibitory action on the accumulative number of AE events, which decreased in logarithmic function, as shown in Figure 14. The cumulative number of AE events of natural specimens reached the maximum with 5.4×10^6 times. In CPST, the cumulative number of AE events show piecewise attenuation characteristics: the first stage is CPST with 0~4.0 h, corresponding to the rapid attenuation stage of AE events. The number of AE events is 3.9×10^6 times at soaking 4.0 h, which is 72.2% of that of natural specimens. The second stage is 4.0~12.0 h, and the number of AE events is 3.3×10^6 times at soaking 12.0 h, which is 61.1% of that of natural specimens. After soaking 24.0 h, the cumulative number of AE events is 3.0×10^6 times, which is 55.6% of that of natural specimens. For different CPSPs, the cumulative number of AE events has similar characteristics with CPST, but on the whole, the decline rate is relatively slow. For the natural water soaking, the AE event number is 4.86×10^6 times and when CPSP is 2.0 MPa, the AE event number is 4.25×10^6 times, which is 78.7% of that of the natural specimen. When CPSP is 4.0 and 6.0 MPa, the AE event number are 70.9% and 68.9% of that of the natural specimen, respectively. Therefore, the reasonable duration of CPS weakening is 2.0~8.0 h and CPSP is 2.0~4.0 MPa.

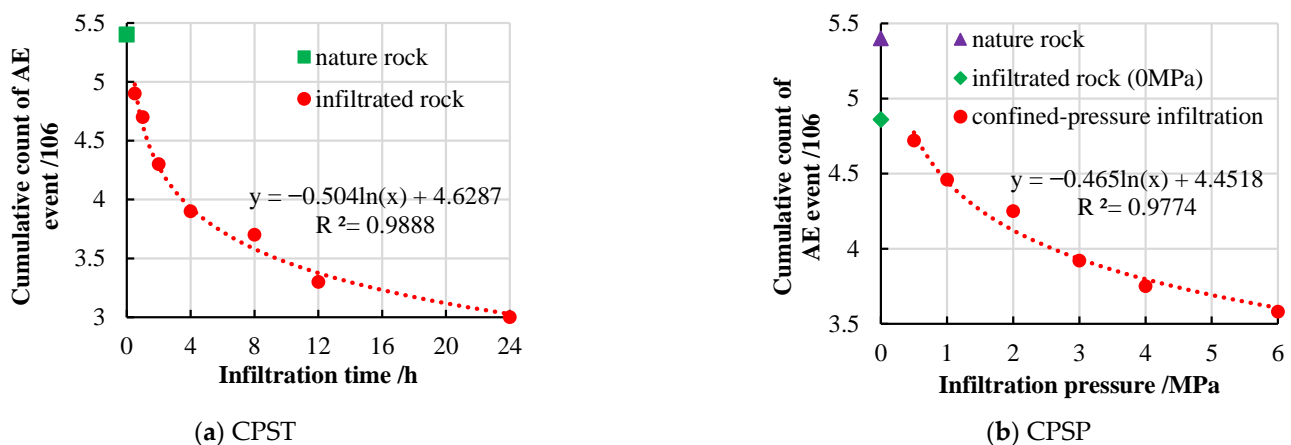


Figure 14. Variation curve of accumulative AE events number under different CPS degrees.

To sum up, the variation of AE accumulation number is consistent with the damage evolution of crack initiation and propagation in loading specimens. Due to the influence of primary fracture and natural damage to a certain extent, the AE event characteristics of sandstone specimens are still different under the same loading conditions. However, the influence trend of CPS degree on the AE event of sandstone is consistent: with the increase in CPS degree, the AE accumulation number decreases greatly, which is due to the clay and other minerals, and the confined water causes micro-structure modification. That is, the greater degree of soaking, the greater damage degree of confined water to the specimen.

According to the description of related literatures, the evolution of AE events in the whole loading process for conventional soaking samples could be divided into quiet period, stable growth, significant growth and sudden change stages [33,41], which is consistent with the change trend of CPS. The growth of moisture contents inhibits the generation of AE signals to a certain extent, and meanwhile delays AE excitation time [19,42]. Compared with conventional soaking, the suppression process of CPS on AE is strengthened, but the weakening effect does not affect AE events and energy concentrated explosion phenomenon when the sample is destroyed [31,43]. Under the CPS with long-term and high-pressure, the starting time of AE signal excitation shows a delayed growth in the increase in CPS parameters. Under high CPS parameters, AE event rate in the stable stage and significant growth stage decreases significantly, and the attenuation intensity of events accumulation is significantly higher than that of conventional soaking. That is, the suppression effect of CPS on AE is stronger than that of conventional conditions, which is one of the research features and innovations of the paper.

3.2.2. Damage Characteristics for Different CPS Degree Based on AE

AE event is the result of fracture development, and the damage increase caused by CPS will lead to the change of constitutive relationship. Therefore, the sandstone damage model under different CPS degrees can be established through damage theory [44,45].

Assuming that the natural specimen is isotropic without initial damage, if the AE events number of complete failure for the specimen section A_m is N_m , the AE event rate n of per-unit area failure is:

$$n = N_m / A_m, \quad (3)$$

The quantitative relationship between the accumulative number of AE events and CPS degree is obtained by fitting:

$$N_d = -A \cdot \ln(t, p) + B, \quad (4)$$

where, A and B are the test fitting parameters. The initial damage variable D of natural sandstone is defined as $D = 0$ and the complete failure $D = 1$. The damage variable D_{AE} related to the degree of CPS based on AE is obtained as follows:

$$D_{AE} = 1 + \frac{[A \cdot \ln(t, p) - B]}{N_m} = \frac{A}{N_m} \cdot \ln(t, p) + \left(1 - \frac{B}{N_m}\right), \quad (5)$$

Variation of the damage coefficient with strain normalization under different CPST and CPSP are shown in Figure 15.

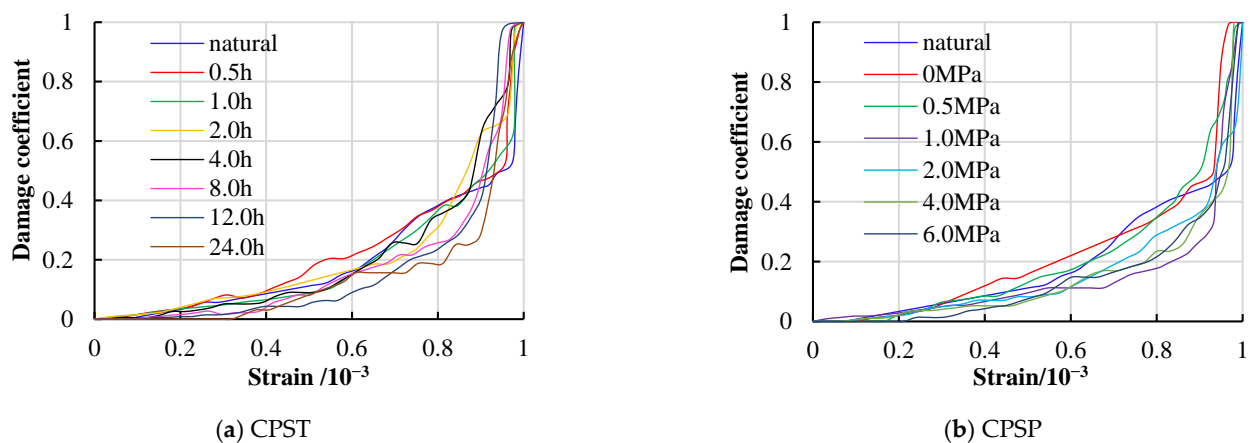


Figure 15. Variation of the damage coefficient and normalized strain of sandstone.

The damage coefficient D_{AE} correlates well with strain normalization and presents three stages, including slow, approximate linear and rapid-abrupt growth on the increasing

of the strain. The inflection point of D_{AE} growth is 25~30% and 85~90% of the failure strain, which is consistent with the strain inflection point of 85~95% reported by Zhou and Wasantha [18,46]. The rapid-abrupt growth of D_{AE} means CPS sandstone has entered the plastic deformation and failure stage. When reaching the inflection point of D_{AE} (85~90%), the range of D_{AE} values is 0.25~0.45 for the CPS sandstone samples. The inflection point in the curve corresponds to more than 90% of the peak strain, but before entering the mutation stage, the damage variable shows a local rapid growth. The stage is determined by the joint action of CPS modification and loading plastic deformation of rock samples. D_{AE} of sandstone under the uniaxial loading differs according to CPST and CPSP. Although CPS has a certain influence on the deformation and damage process of sandstone, the overall variation trend is similar; this is because the loading effect in this change is higher than the CPS modification effect.

Based on the weakening characteristics, the damage variable D_E defined by EM is established [47]:

$$D_E = 1 - \frac{E_s}{E_m}, \quad (6)$$

where E_s is the real-time EM of CPS sandstone; E_m is EM of the natural sandstone.

According to attenuation characteristics of AE event and EM for natural and different CPS degree sandstone, the fitting variation curve of damage quantity with the increase in CPS degree could be obtained:

$$\left\{ \begin{array}{l} \left\{ \begin{array}{l} D_{AE}(t) = 0.0933 \ln(t) + 0.1428 \\ D_{AE}(p) = 0.0776 \ln(p) + 0.1753 \end{array} \right. \\ \left\{ \begin{array}{l} D_E(t) = 0.0828 \ln(t) + 0.1208 \\ D_E(p) = 0.0568 \ln(p) + 0.191 \end{array} \right. \end{array} \right. , \quad (7)$$

With the increase in CPS degree, the damage value of the specimens increased in sections. In CPST, 4.0 h is the inflection point of the growth rate. With soaking 0.5~4.0 h, D increases from 0.093 to 0.278 under AE condition, and D in EM increases from 0.0573 to 0.251, which is the rapid accumulation stage of damage value. With soaking 4.0~24.0 h, D increases from 0.278 to 0.444 under AE condition and D in EM increases from 0.251 to 0.360, in which D growth rate is significantly lower than that of the former with a small increasing rate.

Under the specific CPST, the inflection point of CPSP is 2.0~3.0 MPa. In 0~3.0 MPa, D increases from 0.1 to 0.269 under the AE condition, and D in EM increases from 0.079 to 0.258, in which the growth rate of damage value is larger and more stable. Under the condition of 3.0~6.0 MPa, D increases from 0.269 to 0.311 under the AE condition, and D in EM increases from 0.258 to 0.285, in which the growth rate of damage value is obviously lower than that of the former. The above shows that with the increase in CPSP, the damage degree of sandstone increases correspondingly, but the deterioration degree is lower than that of CPST.

With the increase in CPS degree, D defined by AE is higher than that defined by EM in terms of CPST and CPSP; this is due to the AE event belongs to the crack propagation on the three-dimensional volume of the specimen, while the failure of specimens generally propagates with the single main crack at full height from the aspect of EM. However, before the failure of CPS rock mass, multiple wing cracks will occur near the fracture line (plane) which leads to the number increase in non-penetrating fracture AE events.

Therefore, based on the angle of multiple crack propagation, D defined by the AE event is more suitable to describe the deterioration of CPS rock mass.

3.2.3. Damage Evolution for Different CPS Degree Based on Energy Dissipation

During rock deformation and failure with loading, the sample energy is released and dissipated according with the law of energy conservation. The energy dissipation degree could therefore be employed for analyzing the degree of sandstone damage [48,49].

Assuming that the sample is a closed system, the total energy U varies owing to the response of the external loading, as follows:

$$U = U_E + U_D, \tag{8}$$

where, U_E and U_D are the elastic and dissipation energy, respectively. U and U_{Ei} could be calculated with Equation (9):

$$\begin{cases} U = \sum_{i=0}^n \int_{\varepsilon_i}^{\varepsilon_{i+1}} \sigma_i d\varepsilon = \sum_{i=0}^n (\varepsilon_{i+1} - \varepsilon_i) \cdot \frac{\sigma_i + \sigma_{i+1}}{2} \\ U_{Ei} = \frac{1}{2} \sigma_{i+1} (\varepsilon_{i+1} - \varepsilon_{(i)E}) \approx \frac{\sigma_{i+1}^2}{2E_i} \end{cases}, \tag{9}$$

where ε_i is the strain corresponding stress σ_i , E_i is the elastic modulus at the elastic stage and D_{Ui} is the damage coefficient based on the dissipation energy.

Figure 16 shows the energy distribution relationship under different loading stages. The sandstone damage based on the energy dissipation could therefore be calculated:

$$D_{Ui} = \frac{U_{Di}}{U_D} = \frac{U_i - U_{Ei}}{U_D}, \tag{10}$$

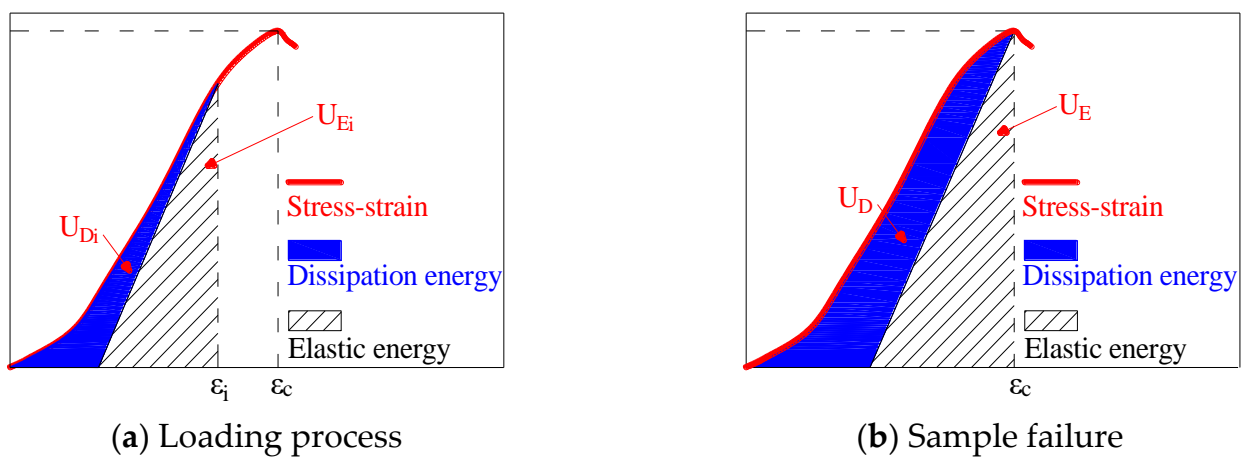


Figure 16. Energy dissipation characteristics during rock deformation.

Variation of the damage coefficient of sandstone based on dissipative energy under different CPST degrees are shown in Figures 17 and 18.

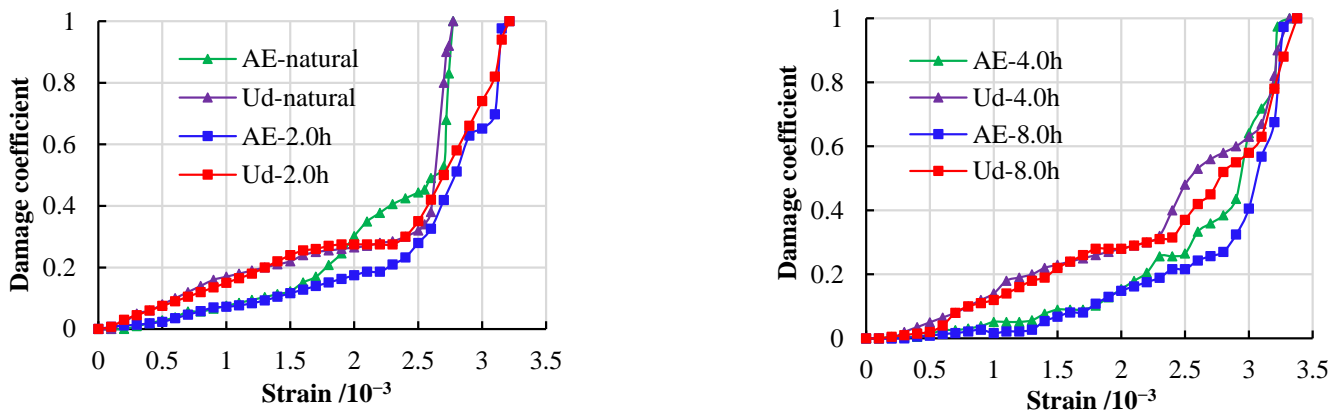


Figure 17. Damage variable of sandstone based on dissipative energy under different CPST (D_{Ud} are damage variables calculated by dissipation energy).

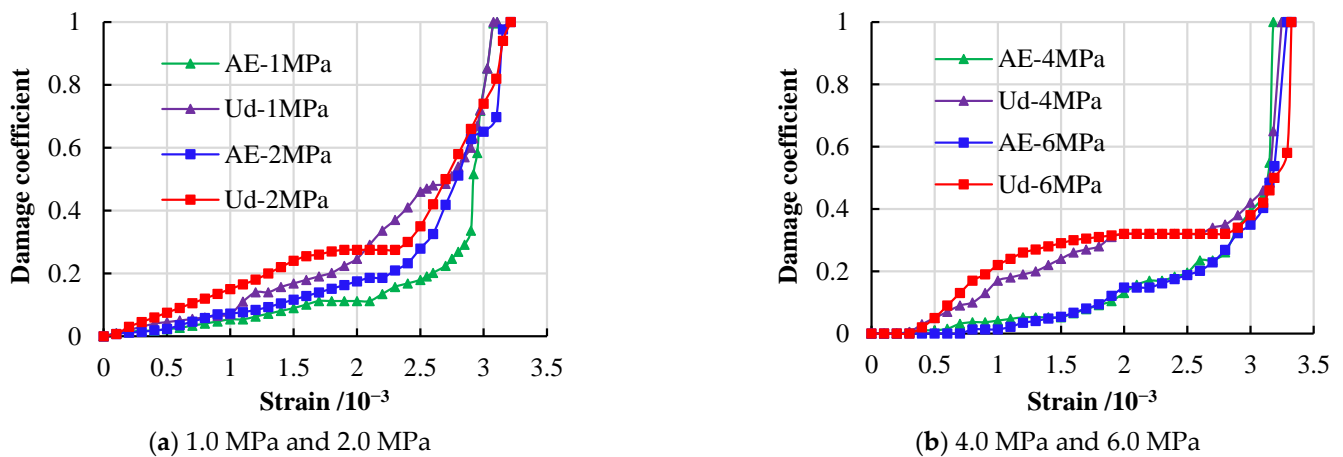


Figure 18. Damage variable of sandstone based on dissipative energy under different CPSP.

The fluctuation growth characteristics of D_{Ud} are consistent with the change trend of the stress-strain curve. In the initial stage of loading (slow and approximate linear growth stage of D_{AE}), D_{Ud} increased significantly and is larger than D_{AE} as a whole, for the dissipation energy is produced due to the closure of internal primary-microcracks accompanied by a small number of AE events. However, the damage degree (D_{Ud} and D_{AE}) develops slowly without substantial change.

During the middle of loading, the closed primary-cracks experienced secondary propagation, and the number of AE events (D_{AE}) increased linearly. However, there is a smooth transition stage of D_{Ud} change in the strain with different span intervals. The slow growth of the stress-strain curve in the initial stage and the approximate linear growth in the middle and later stages will lead to a decrease in D_{Ud} to some extent. Due to the energy dissipation with an irreversible process, the damage coefficient will not decrease in the actual loading process. The difference between D_{Ud} and D_{AE} tends to decrease with the increase in strain. When the loading deformation of the specimen reaches the inflection point of damage change, the difference and discreteness of the damage coefficients D_{Ud} and D_{AE} (dissipation energy) increased under different CPSTs.

When the strain reach 85~95% of the sandstone failure strain (Abrupt inflection-point of rock mass damage growth), the dispersion of the damage coefficients D_{Ud} and D_{AE} (dissipation energy) increases under different CPSTs and a large number of cracks are quickly initiated and propagated, which indicates that the sample is in critical instability state. The damage coefficients calculated with energy dissipation are in accordance with those based on AE. The abrupt growth of D_{Ud} and D_{AE} is an obvious transition point corresponding to 85~95% of the peak strain, which means that the failure of the sample is about to occur.

The related literature describes that the damage of rock mass in the conventional soaking state has gone through the stages of initial compaction closure, stable damage increase and damage acceleration [24,50], and proposes that the quantification of damage variables based on energy dissipation and AE is consistent. The view is consistent with the conclusion of the paper. However, the damage degree of the conventional soaking specimen increases slowly in the stable stage, but it enters the damage acceleration stage ahead of the natural state (before the peak stress), which indicates the critical transition point of damage [16,51]. As for CPS, with the increase in moisture content, the influence point of damage variable growth gradually moves forward, and the corresponding damage growth strain interval gradually expands [52], indicating that the softening effect of CPS is enhanced. For the increase in moisture content caused by CPSP, the damage variable accelerates to accumulate in the stable stage, and the final value in the stable stage is higher than that of the conventional condition. However, under a high CPSP, due to the confined-pressure water activating crack development, a certain degree of internal damage will

be generated, resulting in faster growth of dissipated energy during the loading process. Therefore, the damage variable calculated based on dissipated energy is slightly higher than that of AE. The comparative analysis reflects the unique modification weakening effect of sandstone under the condition of CPS, which is also one of the innovations of the paper.

4. Conclusions

- (1) CPS has an obvious influence on the moisture content and mechanical characteristics of sandstone: with the increase in CPS degree, UCS and EM of sandstone show logarithmic attenuation, and the sandstone varies from brittle to non-brittle failure. The main controlling factor affecting the strength of CPS sandstone is CPST.
- (2) The fracture of specimens with short CPSTs shows concentration and irregularity in the middle-upper regions. The specimens with longer CPSTs penetrate the block axially with a single main crack, showing a homogenized strength weakening effect of CPST. The fracture trajectory of low CPSP specimen is irregular, and the fracture of the specimen with high CPSP is characterized by multi-dimension and small size, which indicates the deterioration characteristics of CPSP.
- (3) The increase in CPS parameters has inhibition effect on AE events in different loading stages, which is consistent with the evolution of internal fracture initiation and propagation. In the damage accumulation stage, AE events show a step-type growth, which is the major growth stage. The cumulative number of AE events attenuates in the form of logarithmic function on the CPST and CPSP, but its response to CPST is more sensitive.
- (4) With the increase in CPS degree, the excitation time of AE event is increasing, which is consistent with the increase in internal fracturing-damage degree. However, the deterioration effect of CPST is better than that of CPSP. Based on the damage theory, the damage variable with different CPS degree based on AE events and energy dissipation of the specimens is established, which have a good consistency to quantify the damage evolution.

Author Contributions: Validation, M.Z.; Writing—original draft, B.C.; Writing—review & editing, B.C. and L.W. All authors have read and agreed to the published version of the manuscript.

Funding: This research was funded by the National Natural Science Foundation of China (Grant No. 52104113), the National Key Research and Development Program of China (Grant No. 2020YFB1314203), the Foundation of Educational Commission of Anhui Province (Grant No. KJ2020A0320), the University-level key projects of Anhui University of science and technology (Grant No. QN2019112) and the Independent Research Fund of the State Key Laboratory of Mining Response and Disaster Prevention and Control in Deep Coal Mines (Grant No. SKLMRDPC19ZZ11).

Institutional Review Board Statement: Not applicable.

Informed Consent Statement: Not applicable.

Data Availability Statement: The data used to support the findings of this study are available from the corresponding author upon reasonable request.

Conflicts of Interest: The authors declare that they have no conflict of interest regarding the publication of this paper.

References

1. Liu, C.Y.; Yang, J.X.; Yu, B. Rock-breaking mechanism and experimental analysis of confined blasting of borehole surrounding rock. *Int. J. Rock Mech. Min. Sci.* **2017**, *27*, 795–801.
2. Masoumi, H.; Horne, J.; Timms, W. Establishing empirical relationships for the effects of water content on the mechanical behavior of Gosford sandstone. *Rock Mech. Rock Eng.* **2017**, *50*, 2235–2242. [[CrossRef](#)]
3. Vasarhelyi, B. Statistical analysis of the influence of water content on the strength of the Miocene limestone. *Rock Mech. Rock Eng.* **2005**, *38*, 69–76. [[CrossRef](#)]
4. Wang, R.J.; Zhang, Q.J.; Li, Y. Deterioration of concrete under the coupling effects of freeze-thaw cycles and other actions: A review. *Constr. Build. Mater.* **2022**, *319*, 126045. [[CrossRef](#)]

5. Yao, Q.L.; Tang, C.J.; Xia, Z.; Liu, X.L.; Zhu, L.; Chong, Z.H.; Hui, X.D. Mechanisms of failure in coal samples from underground water reservoir. *Eng. Geol.* **2020**, *267*, 105494. [[CrossRef](#)]
6. Gu, H.L.; Tao, M.; Li, X.B.; Cao, W.Z.; Li, Q.Y. Dynamic response and meso-deterioration mechanism of water-saturated sandstone under different porosities. *Measurement* **2021**, *167*, 108275. [[CrossRef](#)]
7. Li, Y.; Zhou, Y.; Wang, R.J.; Li, Y.L.; Wu, X.J.; Si, Z. Experimental investigation on the properties of the interface between RCC layers subjected to early-age frost damage. *Cem. Concr. Comp.* **2022**, *134*, 104745. [[CrossRef](#)]
8. Pradhan, S.; Stroisz, A.M.; Fjær, E.; Hans, K.L.; Eyvind, F.S. Stress-induced fracturing of reservoir rocks: Acoustic monitoring and μ CT image analysis. *Rock Mech. Rock Eng.* **2015**, *48*, 2529–2540. [[CrossRef](#)]
9. Yang, J.; Mu, Z.L.; Yang, S.Q. Experimental study of acoustic emission multi-parameter information characterizing rock crack development. *Eng. Fract. Mech.* **2020**, *232*, 107045. [[CrossRef](#)]
10. Zhao, Y.C.; Yang, T.H.; Xu, T.; Zhang, P.H.; Shi, W.H. Mechanical and energy release characteristics of different water-bearing sandstones under uniaxial compression. *Int. J. Damage Mech.* **2018**, *27*, 640–656. [[CrossRef](#)]
11. Yao, Q.L.; Chen, T.; Tang, C.J.; Sedighi, M.; Huang, Q.X. Influence of moisture on crack propagation in coal and its failure modes. *Eng. Geol.* **2019**, *25*, 105156. [[CrossRef](#)]
12. Zhao, Z.H.; Yang, J.; Zhang, D.F.; Peng, H. Effects of wetting and cyclic wetting-drying on tensile strength of sandstone with a low clay mineral content. *Rock Mech. Rock Eng.* **2017**, *50*, 485–491. [[CrossRef](#)]
13. Zhang, P.; Meng, Z.P.; Zhang, K.; Jiang, S. Impact of coal ranks and confining pressures on coal strength, permeability, and acoustic emission. *Int. J. Geomech.* **2020**, *20*, 04020135. [[CrossRef](#)]
14. Qin, X.Z.; Zhou, Y.; He, M.C. Experimental study on mechanical properties and acoustic emission characteristics of water bearing sandstone under stable cyclic loading and unloading. *Shock Vib.* **2020**, *2020*, 9472656. [[CrossRef](#)]
15. Teng, T.; Gong, P. Experimental and theoretical study on the compression characteristics of dry/water-saturated sandstone under different deformation rates. *Arab. J. Geosci.* **2020**, *13*, 517. [[CrossRef](#)]
16. Geng, J.S.; Cao, L.W. Failure analysis of water-bearing sandstone using acoustic emission and energy dissipation. *Eng. Fract. Mech.* **2020**, *231*, 107021. [[CrossRef](#)]
17. Cai, X.; Zhou, Z.L.; Liu, K.W.; Du, X.M.; Zang, H.Z. Water-weakening effects on the mechanical behavior of different rock types: Phenomena and mechanisms. *Appl. Sci.* **2019**, *9*, 4450. [[CrossRef](#)]
18. Zhou, Z.; Cai, X.; Ma, D.; Cao, W.; Chen, L.; Zhou, J. Effects of water content on fracture and mechanical behavior of sandstone with a low clay mineral content. *Eng. Fract. Mech.* **2018**, *193*, 47–65. [[CrossRef](#)]
19. Shen, R.X.; Qiu, L.M.; Zhao, E.L.; Han, X.; Li, H.R.; Hou, Z.H.; Zhang, X. Experimental study on frequency and amplitude characteristics of acoustic emission during the fracturing process of coal under the action of water. *Saf. Sci.* **2019**, *117*, 320–329. [[CrossRef](#)]
20. Zhu, J.; Deng, J.H.; Huang, Y.M.; He, Z.L. Influence of water on the fracture process of marble with acoustic emission monitoring. *KSCE J. Civ. Eng.* **2019**, *23*, 3239–3249. [[CrossRef](#)]
21. Qin, H.; Huang, G.; Wang, W.Z. Experimental study of acoustic emission characteristics of coal samples with different moisture contents in process of compression deformation and failure. *China J. Mech. Eng.* **2012**, *31*, 1115–1120.
22. Xia, D.; Yang, T.H.; Wang, P.T.; Zhang, P.H.; Zhao, Y.C. Experimental study of acoustic emission characteristics of dry and saturated rocks during cyclic loading and unloading process. *J. China Coal Soc.* **2014**, *39*, 1243–1247.
23. Maruvanchery, V.; Kim, E. Effects of water on rock fracture properties: Studies of mode I fracture toughness, crack propagation velocity, and consumed energy in calcite-cemented sandstone. *Geomech. Eng.* **2019**, *17*, 57–67.
24. Wang, W.N.; Yao, Q.L.; Tang, C.J.; Li, H.T.; Liu, H.Y.; Shan, C.H. Mechanical properties damage, fracture evolution, and constitutive model of siltstone under the effect of moisture content. *Geofluids* **2022**, *2022*, 8599808. [[CrossRef](#)]
25. Sun, H.; Ma, L.Q.; Fu, Y.; Han, J.; Liu, S.Y.; Chen, M.M.; Li, Z.; Tian, F. Infrared radiation test on the influence of water content on sandstone damage evolution. *Infrared Phys. Technol.* **2021**, *118*, 103876. [[CrossRef](#)]
26. Zhao, K.; Yang, D.X.; Zeng, P.; Huang, Z.; Wu, W.K.; Li, B.; Teng, T.Y. Effect of water content on the failure pattern and acoustic emission characteristics of red sandstone. *Int. J. Rock Mech. Min.* **2021**, *142*, 104709. [[CrossRef](#)]
27. Luo, D.N.; Xie, Y.Q.; Lu, S.H.; Su, G.S. Experimental study on the effects of water saturation on the microseismic and acoustic emission characteristics of sandstone in different stress states. *Rock Mech. Rock Eng.* **2022**. [[CrossRef](#)]
28. Yao, Q.L.; Wang, W.N.; Li, X.H.; Tang, C.J.; Xu, Q.; Yu, L.Q. Study of mechanical properties and acoustic emission characteristics of coal measures under water-rock interaction. *J. China Univ. Min. Tech.* **2021**, *50*, 558–569.
29. Sun, Q.; Ji, M.; Xue, L.; Su, T.M. The influence of moisture content on the acoustic emission at threshold of rock destruction. *Acta. Geodyn. Geomater.* **2015**, *12*, 279–287. [[CrossRef](#)]
30. Hawkins, A.B.; McConnell, B.J. Sensitivity of sandstone strength and deformability to changes in moisture content. *Q. J. Eng. Geol. Hydrogeol.* **1992**, *25*, 115–130. [[CrossRef](#)]
31. Zhao, K.; Wang, X.; Wang, L.; Zeng, P.; Yang, D.X.; Jin, J.F. Investigation of the crack and acoustic emission behavior evolution of red sandstone subjected to water. *Theor. Appl. Fract. Mech.* **2022**, *120*, 103419. [[CrossRef](#)]
32. Ma, C.Q.; Li, H.Z.; Niu, Y. Experimental study on damage failure mechanical characteristics and crack evolution of water-bearing surrounding rock. *Environ. Earth Sci.* **2018**, *77*, 23–34. [[CrossRef](#)]
33. Li, C.M.; Liu, N.; Liu, W.R. Experimental investigation of mechanical behavior of sandstone with different moisture contents using the acoustic emission technique. *Adv. Civ. Eng.* **2020**, *2020*, 8877921. [[CrossRef](#)]

34. Dong, W.L.; Han, L.J.; Meng, L.D.; Zhu, H.X.; Yan, S.; Xu, C.Y.; Dong, Y.N. Experimental study on the mechanical and acoustic emission characteristics of tuff with different moisture contents. *Minerals* **2022**, *12*, 1050. [[CrossRef](#)]
35. Feng, F.; Chen, S.J.; Wang, Q.; Rostami, J.; Khoreshok, A.A.; Sheng, S.Q.; Bian, Z.; Ding, Y.S. Experimental study on failure characteristics of natural and saturated sandstone under true triaxial unloading and dynamic disturbance condition. *Chin. J. Rock Mech. Eng.* **2022**. [[CrossRef](#)]
36. Gong, C.G.; Wang, W.; Shao, J.F.; Wang, R.B.; Feng, X.W. Effect of water chemical corrosion on mechanical properties and failure modes of pre-fissured sandstone under uniaxial compression. *Acta Geotech.* **2021**, *16*, 1083–1099. [[CrossRef](#)]
37. Wang, H.; Li, Y.; Cao, S.G.; Pan, R.K.; Yang, H.Y.; Zhang, K.W.; Liu, Y.B. Brazilian splitting test study on crack propagation process and macroscopic failure mode of pre-cracked black shale. *China J. Rock Mech. Eng.* **2020**, *39*, 912–926.
38. Ning, J.G.; Wang, J.; Jiang, J.Q. Estimation of crack initiation and propagation thresholds of confined brittle coal specimens based on energy dissipation theory. *Rock Mech. Rock Eng.* **2018**, *51*, 119–134. [[CrossRef](#)]
39. Borisov, V.D. Time and spectrum analysis to study rock failure mechanics. *J. Min. Sci.* **2005**, *41*, 332–341. [[CrossRef](#)]
40. Chen, L.; Zhao, J.; Zheng, Z.Y. Acoustic emission characteristics of compressive deformation and failure of siltstone under different water contents. *Adv. Mater. Sci. Eng.* **2017**, *2017*, 4035487. [[CrossRef](#)]
41. Li, H.R.; Qiao, Y.F.; Shen, R.X.; He, M.C.; Cheng, T.; Xiao, Y.M.; Tang, J. Effect of water on mechanical behavior and acoustic emission response of sandstone during loading process: Phenomenon and mechanism. *Eng. Geol.* **2022**, *294*, 106386. [[CrossRef](#)]
42. Li, H.R.; Shen, R.X.; Qiao, Y.F.; He, M.C. Acoustic emission signal characteristics and its critical slowing down phenomenon during the loading process of water-bearing sandstone. *J. Appl. Geophys.* **2021**, *194*, 104458. [[CrossRef](#)]
43. Codeglia, D.; Dixon, N.; Fowmes, G.J.; Marcato, G. Analysis of acoustic emission patterns for monitoring of rock slope deformation mechanisms. *Eng. Geol.* **2017**, *219*, 21–31. [[CrossRef](#)]
44. Tang, C.A.; Xu, X.H. Evolution and propagation of material defects and Kaiser effect function. *J. Seismol. Res.* **1990**, *13*, 203–213.
45. Wu, C.; Gong, F.Q.; Luo, Y. A new quantitative method to identify the crack damage stress of rock using AE detection parameters. *Bull. Eng. Geol. Environ.* **2020**, *80*, 519–531. [[CrossRef](#)]
46. Wasantha, P.L.; Ranjith, P.G. Water-weakening behavior of Hawkes bury sandstone in brittle regime. *Eng. Geol.* **2014**, *178*, 91–101. [[CrossRef](#)]
47. Xu, Z.L. *Elasticity Mechanics*, 3rd ed.; Higher Education Press: Beijing, China, 2013; pp. 21–27.
48. Xie, H.; Ju, Y.; Li, L. Energy mechanism of deformation and failure of rock masses. *China J. Rock Mech. Eng.* **2008**, *27*, 1729–1740.
49. Xie, H.; Ju, Y.; Li, L. Criteria for strength and structural failure of rocks based on energy dissipation and energy release principles. *China J. Rock Mech. Eng.* **2005**, *24*, 3003–3010.
50. Li, H.R.; He, M.C.; Shen, R.X.; Xiao, Y.M.; Cheng, T. Acoustic emission waveform analysis of sandstone failure with different water content. *Geofluids* **2021**, *2021*, 5290076. [[CrossRef](#)]
51. Yang, K.; Yan, Q.X.; Zhang, C.A.; Wu, W.; Wan, F. Study on mechanical properties and damage evolution of carbonaceous shale under triaxial compression with acoustic emission. *Int. J. Damage Mech.* **2021**, *30*, 899–922. [[CrossRef](#)]
52. Ma, H.F.; Song, Y.Q.; Chen, S.J.; Yin, D.W.; Zheng, J.J.; Shen, F.X.; Li, X.S.; Ma, Q. Experimental investigation on the mechanical behavior and damage evolution mechanism of water-immersed gypsum rock. *Rock Mech. Rock Eng.* **2021**, *54*, 4929–4948. [[CrossRef](#)]